Identification of Autophagosome-associated Proteins and Regulators by Quantitative Proteomic Analysis and Genetic Screens*⒮

Jörn Dengjel‡§¶‖**‡‡, Maria Høyer-Hansen**§§, Maria O. Nielsen‡,
Tobias Eisenberg¶¶, Lea M. Harder‡, Søren Schandorff‡, Thomas Farkas§§,
Thomas Kirkegaard§§, Andrea C. Becker§¶, Sabrina Schroeder¶¶, Katja Vanselow‡,
Emma Lundberg‖‖, Mogens M. Nielsen‡, Anders R. Kristensen‡, Vyacheslav Akimov‡,
Jakob Bunkenborg‡, Frank Madeo¶¶, Marja Jäättelä§§‡‡, and Jens S. Andersen‡‡‡

Autophagy is one of the major intracellular catabolic pathways, but little is known about the composition of autophagosomes. To study the associated proteins, we isolated autophagosomes from human breast cancer cells using two different biochemical methods and three stimulus types: amino acid deprivation or rapamycin or concanamycin A treatment. The autophagosome-associated proteins were dependent on stimulus, but a core set of proteins was stimulus-independent. Remarkably, proteasomal proteins were abundant among the stimulus-independent common autophagosome-associated proteins, and the activation of autophagy significantly decreased the cellular proteasome level and activity supporting interplay between the two degradation pathways. A screen of yeast strains defective in the orthologs of the human genes encoding for a common set of autophagosome-associated proteins revealed several regulators of autophagy, including subunits of the retromer complex. The combined spatiotemporal proteomic and genetic data sets presented here provide a basis for further characterization of autophagosome biogenesis and cargo selection. *Molecular & Cellular Proteomics 11: 10.1074/mcp.M111.014035, 1–17, 2012.*

Macroautophagy (hereafter referred to as autophagy) is an evolutionarily conserved lysosomal pathway involved in the turnover of long-lived proteins, cytoplasm, and whole organelles (1–4). Its deregulation in mice leads to embryonic or perinatal lethality (5, 6), neurodegeneration (7), or cancer (8), emphasizing the physiological importance of this catabolic process. Although autophagy occurs constitutively at a low basal level, starvation, growth factor deprivations, and protein aggregation, as well as other cellular stresses rapidly increase its activity. Under these conditions, autophagy is crucial for generating nutrients or removing damaged cytoplasmic components, thereby serving mainly as a protective cellular response (2).

The autophagic process begins with the nucleation of a flat membrane cistern that enwraps cytoplasmic organelles and/or a portion of the cytosol. The membrane elongates until the edges of the membrane fuse, thereby forming a double membrane structure called an autophagosome, which fuses with endosomes forming an amphisome (9) and subsequently matures to an autolysosome by fusing with lysosomal vesicles. The final degradation of the cargo takes place within autolysosomes, where lysosomal hydrolases digest the luminal content, allowing the recycling of amino acids, nucleotides, and fatty acids (10). The process is controlled by a set of evolutionarily conserved autophagy-related proteins (Atg proteins) initially identified in yeast (11, 12). The protein complex consisting of phosphatidylinositol 3-phosphate kinase class 3, p150 myristylated protein kinase, and beclin 1 (Atg6) is essential for the initial membrane assembly, whereas the following membrane elongation depends on two ubiquitin-like conjugation systems. One of them converts microtubule-associated protein 1 light chain 3 (LC3/Atg8)[1] from its free

[1] The abbreviations used are: LC, light chain; ER, endoplasmic reticulum; mTORC, mammalian target of rapamycin complex; PCP, protein correlation profiling; SILAC, stable isotope labeling by amino acids in cell culture; GFP, green fluorescent protein; eGFP, enhanced GFP; ALP, alkaline phosphatase; HBSS, Hanks' balanced salt solution; siRNA, small interfering RNA; ConA, concanamycin A; Rapa, rapamycin; RHEB, Ras homolog enriched in brain; GABARAPL2, GABA$_A$ receptor-associated protein-like 2; EEF1G, eukaryotic translation elongation factor 1γ; PSM, proteasome subunit.

form (LC3-I) to a phosphatidylethanolamine-conjugated form (LC3-II), which associates with both membranes of the autophagosome (13). This process is frequently used as an autophagy marker because the change in the LC3 staining pattern from diffuse to dotted can be readily visualized.

Autophagy is generally considered an unselective bulk degradation pathway. However, under certain conditions, autophagosomes have been suggested to selectively remove, for example, damaged mitochondria (14), endoplasmic reticulum (ER) (15), peroxisomes (16), ribosomes (17), and the midbody ring at the end of cytokinesis (18). Moreover, our recent proteomic analysis of starved cells shows that cellular proteins decrease in an ordered fashion depending on their subcellular localization (19). Thus, autophagy may also serve as a specific degradation system, similar to the proteasome, which recognizes ubiquitin-coupled proteins for degradation (20). Even though the ubiquitin-proteasome system and autophagy have long been viewed as complementary degradation systems with no point of intersection, it was shown recently that autophagy can act compensatorily when the ubiquitin-proteasome system is impaired in *Drosophila melanogaster* (21). These data suggest that there might be a link between the two major cellular proteolysis pathways (22–24).

The aim of this study is to identify proteins associated with the mature autophagosome and to compare the protein composition of autophagosomes induced by different stimuli. For this purpose, we analyzed autophagosomes isolated from MCF7 breast cancer cells following amino acid starvation or treatment with either rapamycin (an inhibitor of the mammalian target of rapamycin complex 1 (mTORC1)) or concanamycin A (an inhibitor of the lysosomal H^+-ATPase) by quantitative MS-based proteomics (25) relying on protein correlation profiling (PCP) (26) and stable isotope labeling by amino acids in cell culture (SILAC) (27, 28). We identified 728 putative autophagosome-associated proteins from a background of co-purifying proteins. Of these, only a total of 94 proteins were common to all stimuli. To validate that the co-migrating proteins were derived from autophagosomes, we performed GFP pulldowns directed against a GFP-tagged version of the autophagosomal marker LC3 and tested subcellular localization by fluorescent microscopy for selected candidate proteins. To test whether the common autophagosome-associated proteins functioned as autophagy regulators, we turned to yeast genetics and screened the available yeast strains with mutations in the corresponding genes for changes in autophagy by the alkaline phosphatase (ALP) assay (29) identifying inter alia the retromer complex. Human cells depleted for the novel autophagy regulators identified in the yeast screen were subsequently analyzed for changes in autophagic flux by cell assays detecting the turnover of autophagosome-associated proteins (30, 31). The data presented provide a quantitative proteomic characterization of autophagosomes identifying a set of autophagosome-associated proteins and regulators.

EXPERIMENTAL PROCEDURES

Cell Culture—For SILAC experiments MCF7-eGFP-LC3 cells (49) were cultured in Dulbecco's modified Eagle's medium (Invitrogen) supplemented with penicillin/streptomycin (100 units/ml, 100 μg/ml), glutamine, and 10% dialyzed fetal calf serum (Invitrogen) and labeled with either L-lysine and L-arginine (Lys^0, Arg^0), L-lysine-$^2H_4$ and L-arginine-$^{13}C_6$ (Lys^4, Arg^6), or L-lysine$^{13}C_6$-$^{15}N_2$ and L-arginine$^{13}C_6$-$^{15}N_4$ (Lys^8, Arg^{10}) (Cambridge Isotope Laboratories, Andover, MA; Sigma-Aldrich). Otherwise the cells were grown in Dulbecco's modified Eagle's medium or RPMI (Invitrogen) with 10% FCS and penicillin/ streptomycin. The cells were treated with concanamycin A, rapamycin, and etoposide (all from Sigma-Aldrich) or washed three times in PBS before they were amino acid-starved in HBSS containing calcium, magnesium, and 1 g of glucose/liter (Invitrogen).

Transfections—Fusion constructs of DsRed and RHEB or FKBP1A were generated using vectors pDsRed-C1 and -N1, respectively, (Clontech). RHEB and FKBP1A cDNAs were purchased from imaGenes (Berlin, Germany), and fusion constructs were sequence checked. Stable cell lines were generated by liposomes transfection using Metafectene™ (Biontex, Martinsried, Germany). During transient transfections FuGENE 6 (Roche Applied Science) was used as a transfection agent according to the manufacturer's instructions. siRNA sequences corresponding to the human cDNA sequence are listed in the supplemental material. The cells were transfected with 50 nM siRNA employing Oligofectamine™ (Invitrogen).

Immunodetection—The primary antibodies used for immunoblot analysis are listed in the supplemental "Experimental Procedures." The appropriate peroxidase-conjugated secondary antibodies were from Dako A/S (Glostrup, Denmark) and Vector Laboratories (Burlingame, CA), and the ECL immunoblotting reagents were from Amersham Biosciences.

The cells were fixed and stained applying standard procedures (49). For detection of DsRed fusion proteins, the cells were fixed and permeabilized in 3.7% paraformaldehyde for 7 min followed by methanol overnight. The primary antibodies are listed in supplemental "Experimental Procedures." The respective fluorescent secondary antibodies were from Molecular Probes or Jackson Immunolabs. The images were obtained using either a Zeiss LSM 510 META confocal laser scanning microscope or Zeiss Axiovert 100M confocal laser scanning microscope (Carl Zeiss, Jena, Germany).

Detection of Autophagosomes—Percentages of cells with eGFP-LC3 translocation into dots (a minimum of 100 cells/sample) were counted blindly in cells fixed in 3.7% formaldehyde and 0.19% picric acid (v/v) applying a Zeiss Axiovert 100M confocal laser scanning microscope (Carl Zeiss).

Autophagic Flux—The autophagic flux was measured applying a luciferase-based assay as described previously (30).

Proteasome Activity Assay—The proteasome activity was measured using the 20 S proteasome activity assay kit from Chemicon International (catalog number APT280; Temecula, CA), and the protein levels were measured using the Bio-Rad Dc protein assay kit (Bio-Rad) according to the manufacturer's instructions (supplemental "Experimental Procedures").

Autophagy Measurements in Yeast—The experiments were carried out with BY4741 (MATa *his3Δ1 leu2Δ0 met15Δ0 ura3Δ0*) and respective null mutants, obtained from Euroscarf (growth conditions described in the supplemental "Experimental Procedures"). For induction of autophagy by nitrogen starvation, the cells were inoculated from fresh overnight cultures to 0.4 A_{600} (~4 × 10⁶ cells/ml) in Synthetic Complete Dextrose, grown for 4–5 h to mid-log phase reaching ~1.5 A_{600}, washed twice in double distilled H_2O, and incubated in SD-N medium at 1 A_{600} for 3 h. For induction of autophagy by rapamycin treatment, the cells were grown to mid-log phase (~1

A_{600}) as above, and rapamycin (AG Scientific) was added to the culture to a final concentration of 0.5 μg/ml preceding 3 h of incubation.

Autophagy was determined in cellular extracts of 1-ml culture aliquots by ALP activity according to Ref. 50 using respective strains transformed with and selected for stable insertion of pTN9 HindIII fragment containing the cytosolic form of Pho8p (Pho8pΔN60). For details see the supplemental "Experimental Procedures".

Autophagosome Purification and Mass Spectrometry—Autophagosome purification was modified from the protocol described in Ref. 51 (for details see the supplemental "Experimental Procedures"). The PCP-SILAC background fractions (Lys^0/Arg^0) were combined and spiked in a 1:1 ratio to the respective (Lys^4/Arg^6) PCP SILAC fractions (52). The resulting fractions were dilluted 1:1 in Homogenization Medium and pelleted at 31,000 $\times$ g. The pellets were resuspended in SDS loading buffer and reduced and alkylated. Protein mixtures were separated by SDS-PAGE (4–12% Bis-Tris gradient gel, NuPAGE; Invitrogen) and in-gel digested with trypsin. In the GFP tag enrichment experiment, vesicles were enriched by centrifugation followed by GFP antibody pulldown (supplemental Fig. S3). The proteins were digested in solution with trypsin and the peptides separated by ion exchange chromatography. The resulting peptide mixtures were analyzed by online C18 reversed phase nanoscale liquid chromatography tandem mass spectrometry essentially as described (53) (for details see the supplemental "Experimental Procedures").

Assigning Peptide Sequences Using MASCOT and Quantitation Using MSQuant—Raw MS2 spectra were centroided and merged into a single peak list file using the in-house-developed software DTASupercharge (default values; version 1.19, msquant.sourceforge.net) and searched against the human MSIPI database (v. 3.34 with 68404 entries) (54) using MASCOT 2.0 (Matrix Science, London, UK) basically as described (19) and the following parameters: carbamidomethyl-cysteine was set as fixed modification, methionine oxidation, deamidation of asparagine and glutamine, and protein amino-terminal acetylation were set as variable modifications. Double or triple SILAC were chosen as quantification mode. Two miss cleavages were allowed, enzyme specificity was trypsin, precursor mass accuracy had to be within 30 ppm for FT-data and 7 ppm for Orbitrap data, and the fragment spectra mass accuracy was set at 0.6 Da. The identified peptides were recalibrated using MSQuant (55), and the results were combined using MGFcombiner (version 1.05) and searched again using MASCOT 2.0 with the above mentioned parameters, except that the precursor mass tolerance was set to 5 ppm. To determine the number of false positive peptide hits, the data were searched against a full-length human MSIPI decoy database, and the MASCOT peptide score was adjusted to yield a number of false positive peptide identifications of less than 1% (calculated as follows: false positive rate (%) = reverse hits $\times$ 2 $\times$ 100/forward hits). For a protein to be counted as identified, a minimum of two unique peptides (bold red hits, minimum length of 7 amino acids) had to be sequenced and to fulfill the determined criteria. To yield the maximum number of peptides per identified protein, the data were researched against decoy databases consisting of the identified proteins only considering proteins that were identified using a full-length decoy database and that did pass the stringent identification criteria stated above. Thus, the peptide MASCOT identification score yielding less than 1% false positive could be dropped to 15, resulting in considerably more peptide IDs/protein. PCP SILAC profiles were calculated using all bold red and parenthesized peptides. The proteins were only included if respective peptides were sequenced in each of the six fractions yielding six data point profiles. In a few exceptions, the peptides were inserted based in on elution time predicted from the analyses of neighbor fractions. The peptides were quantified by MSQuant (55) using extracted ion chromatograms of the monoisotopic signals. For

cluster analyses, the protein ratios were normalized using the base 2 logarithm.

The GFP pulldown data was processed and analyzed using MaxQuant (version 1.0.13.13) (56) and Mascot (version 2.3). The Quant module of MaxQuant was used with parameters set as follows: Arg^6/Lys^4 and Arg^{10}/Lys^8 as triple SILAC labels, a maximum of two missed cleavages, filtering of MS/MS spectra to retain only the six most intense peaks/100 Da, and MS/MS mass tolerance of 0.5 Da. Variable modifications were methionine oxidation and protein amino-terminal acetylation. Cysteine carbamidomethylation was a fixed modification. Protein and peptide FDR of 0.01, PEP based on Mascot score, minimum peptide length of 6, minimum score of 7, minimum unique sequence of 1, minimum peptides of 1, use of both unmodified and modified peptides for protein quantification, and use of both razor and unique peptides for quantification with a minimum ratio count of 2.

Clustering of Profiles and Comparative Analysis—The protein profiles were clustered using GProX (57) to identify proteins with profiles similar to known autophagosomal proteins. Clustering was done using the fuzzy c-means algorithm (38), which is a soft clustering algorithm being noise robust and indicating how well protein profiles are represented by respective clusters. The Fuzzy c-means parameter m varied between 1.25 (Rapa), 2.5 (HBSS), and 3.0 (ConA) for the three stimuli to compensate for differences in resolution of the data and to ensure minimal size of autophagosomal clusters. Proteins were considered to being autophagosomal if they clustered with MAP1LC3, p62, and GABA$_A$ receptor-associated protein-like 2 (GABARAPL2). To test the validity of the clusters, it was required that major complexes like the ribosome, the exosome, and the proteasome located to a single cluster (see the supplemental "Experimental Procedures").

RESULTS

Quantitative Mass Spectrometric Analysis of Autophagosomes by PCP-SILAC—Extensive efforts have focused on the description of protein networks involved in autophagy signaling (32). However, the protein composition of autophagosomes is still largely unknown, and only a few autophagosome-associated proteins have been identified (33, 34). One of them is the frequently used autophagosomal marker LC3-II. In this study, we took advantage of MCF7 breast carcinoma cells stably expressing LC3 fused to enhanced green fluorescent protein (eGFP-LC3) to follow the accumulation of autophagosomes after 7-h treatments by three well characterized stimuli, *i.e.* amino acid starvation, rapamycin, and concanamycin A (31) (Fig. 1, *A* and *B*). This experimental system was then used to characterize the stimuli-dependent protein composition of autophagosomes and the function of the identified candidate proteins using a combination of quantitative proteomics and genetic analyses (Fig. 1*A*).

To distinguish autophagosomal candidate proteins from nonspecific co-purifying proteins, we applied the PCP-SILAC method (35, 36). This method is based on the assumption that proteins residing in the same organelle will have similar distributions through a density gradient. As outlined in Fig. 1*C*, two preparation of autophagosomes were isolated in parallel from MCF7-eGFP-LC3 cells labeled with different combinations of isotope-encoded lysine and arginine (37). Fractions collected after the final iodixanol density gradient centrifugation (1.05–1.25 g/ml iodixanol) were tested for the presence of organellar markers and known autophagosomal proteins by
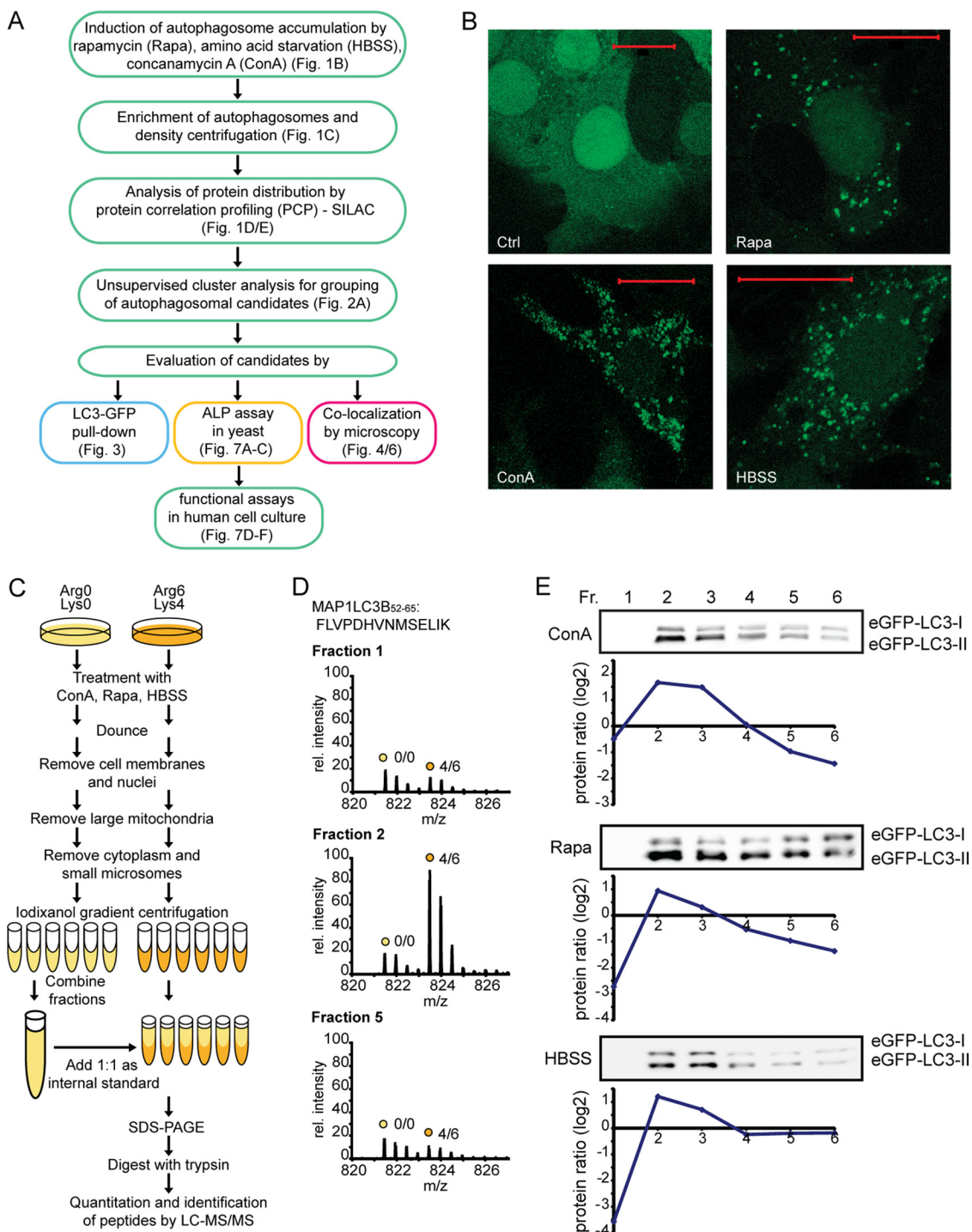
FIG. 1. **PCP-SILAC analyses of autophagosomes.** *A*, schematic outline of experiments performed to identify and characterize proteins associated with autophagosomes. *B*, accumulation of autophagosomes in MCF7-eGFPLC3 cells was tested by fluorescent microscopy. Representative confocal images (*scale bars*, 20 μm) are shown for cells left untreated (control, *Ctrl*) or treated with 1 μM Rapa and 2 nM ConA or starved in HBSS for 7 h. Notably, the cells expressing a mutated form of eGFP-LC3-G120A unable to become lipid-conjugated did not form dots upon stimulation (data not shown), strongly suggesting that the dots observed are autophagosomes rather than unspecific aggregates. *C*, to identify autophagosome-associated proteins using the PCP-SILAC methods, the cells were isotope-labeled and subsequently treated for 7 h with 2 nM ConA. Autophagosomes were purified by gradient centrifugation, six fractions were collected, and the Lys[0]/Arg[0] fractions were combined, yielding an internal standard mixture of proteins over the gradient. This internal standard was distributed in a 1:1 ratio to the original Lys[4]/Arg[6] labeled fractions, and the combined samples were separated by SDS-PAGE, in-gel digested by trypsin, and analyzed by MS. The experiment was repeated using 100 nM rapamycin and starvation in HBSS as stimuli. Applying this setup, we were able to identify 7935 proteins

Western blot analysis (Fig. 1*E* and supplemental Fig. S1). For peptide isotope ratio determination, six fractions containing autophagosomal markers from the unlabeled cells were combined to generate a common internal standard that was equally distributed into the corresponding six fractions from the labeled cells. Proteins in these six samples were then analyzed by LC-MS, and the resulting data were used to determine the relative enrichment of proteins in each fraction (Fig. 1*D*). The protein enrichment profile of LC3 and Western blot analyses of eGFP-LC3 indicated that the majority of autophagosomes appeared in fractions 2 and 3 regardless of the stimulus (Fig. 1*E*). In contrast, marker proteins for other organelles showed clearly distinct profiles (supplemental Fig. S1*B*). In total, 7935 proteins were identified in single representative PCP-SILAC experiments for each of the three stimuli (from a total set of one concanamycin A experiment, two rapamycin experiments, and two starvation experiments; supplemental Fig. S2). Complete protein enrichment profiles were obtained for 4516 proteins detected in all six fractions (supplemental Fig. S2 and Tables S1–S3). These 4516 proteins were grouped into three clusters per experiment based on their profiles using the noise robust fuzzy c-means algorithm (38). Cluster A proteins peaked in fractions 2 and 3 and included known autophagosomal proteins such as LC3, p62 (SQSTM1), and GABARAPL2 (Figs. 2*A* and supplemental Fig. S2). Cluster B contained proteins that also peaked in fractions 2 and 3 but showed an additional rise in fraction 6. Cluster C included proteins that peaked in fraction 5 and 6 and were regarded as nonspecific co-purifying proteins. Autophagosomal clusters (cluster A) from concanamycin A-treated, rapamycin-treated, and starved cells contained 238, 359, and 482 protein profiles, respectively (supplemental Tables S1–S3). These profiles represent 728 different proteins, of which 94 were found in the autophagosomal cluster for all three stimuli (Table I and Fig. 2*B*). In support of the PCP-SILAC method, we identified 42 of the 94 proteins in cluster A that were known autophagosomal proteins or recently reported interaction partners of autophagy-related proteins (Table I and supplemental Table S4). Identification of autophagy regulators such as FK506-binding protein 1 (FKBP1A) and Ras homolog enriched in brain (RHEB) suggests that they operate at the autophagosome scaffold.

Using Gene Ontology (39), we analyzed the subcellular localization of proteins detected in the same clusters independent of the autophagosome-stimulating treatment. Because proteins may carry more than one Gene Ontology term, the sum of all annotated proteins may be higher than 100%.

The majority of proteins in the autophagosomal cluster A were annotated as cytoplasmic/cytosolic (Fig. 2*C*). In addition to the cytoplasmic/cytosolic proteins, cluster B was enriched in proteins from the endosomal compartment, ER, Golgi, cellular membranes, and ribosomes, whereas cluster C contained mainly membrane, extracellular, and ER proteins. Hence, we were able to distinguish different vesicular compartments by our PCP-SILAC approach and identified cluster A as the autophagosomal cluster.

Quantitative Mass Spectrometric Analysis of Immunopurified Autophagosomes—To further support the enrichment of autophagosome-associated proteins in cluster A and to distinguish them from co-migrating vesicular structures, we purified autophagosomes from MCF7-eGFP-LC3 cells by immunoprecipitation using an anti-GFP antibody (Fig. 3*A*) (33). Cell extracts were depleted for the free pool of LC3 by centrifugation to minimize binding of the nonautophagosomal pool of proteins. Specific autophagosome-associated proteins were determined by SILAC-based mass spectrometry comparing the relative abundance of proteins isolated from untreated and starved cells (Fig. 3*A*). Starvation induces a high autophagic flux (see Fig. 5*C*) challenging the identification of protein enrichment in affinity-purified autophagosomes. Therefore, a third condition was analyzed: starved cells treated additionally with concanamycin A, which leads to a pronounced accumulation of autophagosomes by blocking lysosomal degradation (Fig. 3*A* and data not shown). Contaminating proteins should be equally abundant in all three conditions and hence have 1:1:1 ratios, whereas autophagosomal proteins such as LC3 and p62 display higher ratios in the ConA sample where autophagosomes accumulate (supplemental Table S5). Indeed, common cluster A proteins show a nonrandom distribution and are significantly enriched compared with cluster B and C proteins supporting autophagosome association for cluster A proteins ($p < 0.001$; Fig. 3, *B* and *C*, and supplemental Fig. S3 and Table S5). A second eGFP-IP was performed on cells either starved or treated with rapamycin and ConA and confirmed the enrichment of cluster A proteins (supplemental Table S5). In total, 65 common cluster A proteins were identified in the eGFP pulldowns (Table I). Furthermore, immunofluorescence microscopy validated the co-localization of the three cluster A proteins p62, RHEB, and FKBP1A with LC3 following all three stimuli (Fig. 4 and supplemental Figs. S4 and S5).

Stimulus-dependent and Kinetic Differences in the Autophagosome Proteome—Autophagy can be induced by a broad range of stress stimuli that involve diverse signaling pathways. To evaluate whether different stimuli impart

by 180 LC-MS/MS experiments of 140-min length each. *D*, mass spectra of the LC3 peptide FLVPDHVNMSELIK showing isotope envelopes of signal doublets, which represent its relative enrichment over the gradient in the PCP-SILAC experiment. The *colored circles* represent the respective SILAC label. *E*, comparison between PCP-SILAC protein enrichment profiles and anti-eGFP Western blot analyses of biological replicates from cells starved (HBSS) or treated with ConA or rapamycin for 7 h. Shown are eGFP-LC3-I (*upper row*) and eGFP-LC3-II (*lower row*) bands. Both experiments indicate that autophagosomes peak in fractions 2 and 3. *Fr.*, fraction.
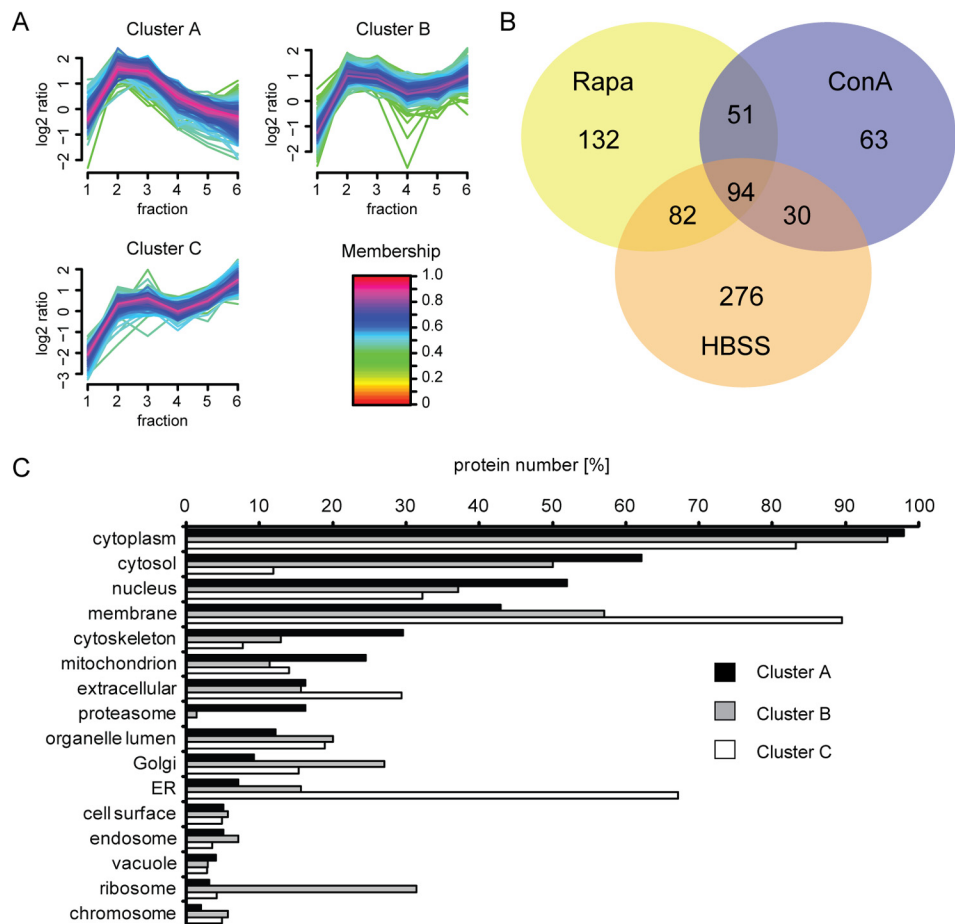
FIG. 2. **Cluster analysis of PCP-SILAC data.** *A*, cluster analysis of protein enrichment profiles obtained from the PCP-SILAC experiment of ConA-treated cells. Three clusters were generated consisting of 238, 273, and 285 proteins, respectively, using the fuzzy c-means algorithm. Cluster A contains all identified proteins known to be associated with autophagosomes. Cluster membership values of protein enrichment profiles are indicated by the *color scale*. Cluster analysis of protein enrichment profiles from the PCP-SILAC experiments of HBSS- and Rapa-treated cells are shown in supplemental Fig. S2. *B*, Venn diagram of the cluster A proteins identified from the HBSS-, Rapa-, and ConA-treated cells. Whereas 94 proteins were in common for the three stimuli, the majority of proteins were detected by only one or two stimuli. Shown are three representative data sets of five biological replicates. *C*, subcellular localization of common proteins in clusters A–C based on Gene Ontology.

changes in the composition and abundance of proteins associated with autophagosomes, we compared proteins identified in cluster A between the different PCP-SILAC experiments and performed additional comparative and temporal quantitative experiments. Interestingly, PCP-SILAC revealed stimuli-dependent groups of proteins in the autophagosomal clusters A (Fig. 5*A*). For instance, starvation triggered autophagosomes associated with plasma membrane proteins and, similar to rapamycin, vesicular proteins. These classes of proteins were largely absent in autophagosomes purified from concanamycin A-treated cells. We compared protein abundances directly between autophagosomes isolated from starved, rapamycin-treated, and concanamycin A-treated cells. Proteins known to be involved in autophagy, such as LC3, p62, and GABARAPL2, were significantly less abundant in autophagosomes from starved cells as compared with rapamycin- and concanamycin A-induced autophagosomes

(Fig. 5*B* and supplemental Table S6). This suggests that starvation induces the highest level of autophagic flux as confirmed by the rapid depletion of p62 in starved cells (Fig. 5*C*). Conversely, a few proteins comprising several members of the annexin family were most abundant in autophagosomes from starved cells (Fig. 5*D*). Proteasomal proteins on the other hand were present in similar amounts regardless of the stimulus (Fig. 5*B*).

To investigate the recruitment dynamics of proteins to the autophagosome, we starved cells for 3, 6, and 12 h, isolated autophagosomes, and analyzed the changes in the abundance of autophagosome-associated proteins (supplemental Table S7). p62 decreased most rapidly within the time frame of analysis, whereas proteasomal proteins (PSMB1) and, for example, eukaryotic translation elongation factor 1γ (EEF1G) showed a slight increase (Fig. 5*E*). Taken together, this suggests that autophagosomes are highly dynamic struc-

TABLE I

Autophagic activity screen in yeast strains defective of the orthologs of the genes encoding for the common autophagosome associated proteins

The common proteins localizing to autophagosomes of MCF7 cells independent of the stimuli.

Protein	Gene ID (human)	Yeast ortholog	Autophagic activity[a]		Reference[d]	eGFP-IP[e]
			Nitrogen starvation[b]	Rapamycin[c]		
Alanyl tRNA synthetase	AARS	ALA1[f]				+
Annexin A4	ANXA4				32[g]	
Annexin A5	ANXA5				32[g]	++
Archain 1	ARCN1	RET2[f]				++
ADP-ribosylation factor 1	ARF1	ARF2	126.1 ± 16.0		32[g]	++
Argininosuccinate synthase 1	ASS1	ARG1	115.8 ± 11.6			++
5-Aminoimidazole-4-carboxamide ribonucleotide formyltransferase/IMP cyclohydrolase	ATIC	ADE17	99.7 ± 13.5		32[g]	
Biliverdin reductase B	BLVRB					++
γ-Glutamyl cyclotransferase	C7orf24					
Calcyclin-binding protein	CACYBP				32[g]	+
Calpain, small subunit 1	CAPNS1				32[g]	+
Chaperonin containing TCP1, subunit 2	CCT2	CCT2[f]				++
Chaperonin containing TCP1, subunit 5	CCT5	CCT5[f]				++
Chaperonin containing TCP1, subunit 8	CCT8	CCT8[f]				++
Cofilin 1	CFL1	COF1[f]				++
Chromatin modifying protein 6	CHMP6					
Coatomer protein complex, subunit ζ1	COPZ1	RET3[f]				+
Copine III	CPNE3					
Cellular retinoic acid-binding protein 2	CRABP2					+
Cystatin B	CSTB					
Destrin	DSTN					++
Eukaryotic translation elongation factor 1γ	EEF1G	TEF4	**56.2 ± 16.3**	84.3 ± 19.1		++
Eukaryotic translation elongation factor 2	EEF2	EFT2	104.5 ± 23.2			++
Enolase 1	ENO1	ENO1	95.8 ± 38.0		34[h]	++
Fatty acid synthase	FASN	CEM1	101.4 ± 14.2			++
Fructose-1,6-bisphosphatase 1	FBP1	FBP1	99.2 ± 16.9		34[h]	+
FK506-binding protein 4, 59 kDa	FKBP4	FPR1	86.2 ± 17.0		32	+
Glucose-6-phosphate dehydrogenase	G6PD	ZWF1	108.3 ± 12.8			++
GABA_A receptor-associated protein-like 2	GABARAPL2	ATG8	**26.1 ± 21.4**	**44.7 ± 26.3**	58	+
GDP dissociation inhibitor 2	GDI2				32[g]	++
Guanine nucleotide-binding protein, β polypeptide 2-like 1	GNB2L1	ASC1	**148.0 ± 21.5**	**210.7 ± 43.1**		+
Glucose phosphate isomerase	GPI	PGI1[f]				++
Glutathione reductase	GSR	GLR1	90.7 ± 9.1			
Hypoxanthine phosphoribosyltransferase 1	HPRT1					+
Heat shock protein 90-kDa α, class A member 1	HSP90AA1	HSC82	100.0 ± 15.9			++
Heat shock protein 90-kDa α, class B member 1	HSP90AB1	HSP82	90.6 ± 6.8			++
Heat shock 27-kDa protein 1	HSPB1					++
KIAA1609	KIAA1609					++
LIM and SH3 protein 1	LASP1				32[g]	+
Lectin, galactoside-binding, soluble, 3	LGALS3					++
Microtubule-associated protein 1 light chain 3β	MAP1LC3B	ATG8	**26.1 ± 21.4**	**44.7 ± 26.3**	58	
Malate dehydrogenase 1	MDH1				34[h]	
Macrophage migration inhibitory factor	MIF					++
Purine nucleoside phosphorylase	NP	PNP1	**46.0 ± 5.9**	**30.1 ± 10.6**		
Aminopeptidase, puromycin-sensitive	NPEPPS	AAP1	101.4 ± 34.4		32[g]	+
Platelet-activating factor acetylhydrolase 1b, catalytic subunit 3	PAFAH1B3					
Poly(rC)-binding protein 1	PCBP1	PBP2	103.4 ± 8.8		33	++
Phosphatidylethanolamine-binding protein 1	PEBP1				32[g]	+
Profilin 1	PFN1	PFY1[f]				++
Profilin 2	PFN2					
Phosphogluconate dehydrogenase	PGD	GND1	111.5 ± 25.2			

TABLE I—*continued*

Protein	Gene ID (human)	Yeast ortholog	Autophagic activity[a]		Reference[d]	eGFP-IP[e]
			Nitrogen starvation[b]	Rapamycin[c]		
Phosphoglycerate dehydrogenase	PHGDH	SER33	98.7 ± 31.8			++
Pyruvate kinase, muscle	PKM2	CDC19[f]				++
Peptidylprolyl isomerase A	PPIA	CPR1	94.9 ± 16.3		34[h]	++
Protein phosphatase 3, catalytic subunit, α isoform	PPP3CA	CMP2	102.7 ± 11.1			+
Peroxiredoxin 1	PRDX1	TSA1	96.8 ± 11.6		34[h]	++
Peroxiredoxin 2	PRDX2	TSA1	96.8 ± 11.6		34[h]	++
Peroxiredoxin 6	PRDX6	PRX1	90.9 ± 6.0		34[h]	++
Proteasome subunit, α type, 2	PSMA2	PRE8[f]			45[g]	+
Proteasome subunit, α type, 3	PSMA3	PRE10[f]			45[g]	
Proteasome subunit, α type, 5	PSMA5	PUP2[f]			45[g]	+
Proteasome subunit, α type, 6	PSMA6	SCL1[f]			45[g]	+
Proteasome subunit, α type, 7	PSMA7	PRE6[f]			45[g]	+
Proteasome subunit, β type, 1	PSMB1	PRE7[f]			45[g]	
Proteasome subunit, β type, 2	PSMB2	PRE1[f]			45[g]	+
Proteasome subunit, β type, 3	PSMB3	PUP3[f]			45[g]	
Proteasome subunit, β type, 4	PSMB4	PRE4[f]			45[g]	
Proteasome subunit, β type, 5	PSMB5	PRE2[f]			45[g]	
Proteasome subunit, β type, 6	PSMB6	PRE3[f]			45[g]	
Proteasome subunit, β type, 7	PSMB7	PUP1[f]			45[g]	
Proteasome 26 S subunit, ATPase, 6	PSMC6	RPT4[f]			45[g]	
Proteasome activator subunit 1	PSME1				45[g]	++
Proteasome activator subunit 2	PSME2				45[g]	++
Ras homolog enriched in brain 1	RHEB1	RHB1	36.3 ± 11.1	37.2 ± 4.2	59[g]	
Ribosomal protein S21	RPS21	RPS21B	85.5 ± 4.3			
Ribosomal protein SA	RPSA	RPS0A	90.8 ± 32.7			+
S100 calcium-binding protein A11	S100A11					++
S100 calcium-binding protein A13	S100A13					
SH3 domain binding glutamic acid-rich protein like	SH3BGRL					
Sequestosome 1	SQSTM1				41	++
Spermidine synthase	SRM	SPE3	119.1 ± 23.1		32[g]	
Stress-induced-phosphoprotein 1	STIP1	STI1	113.4 ± 24.3			++
Tumor protein D52-like 2	TPD52L2					++
Triosephosphate isomerase 1	TPI1	TPI1[f]				++
Tubulin, β	TUBB	TUB2[f]				++
Tubulin, β 2C	TUBB2C					++
Thioredoxin	TXN	TRX2	101.2 ± 29.7			+
Thioredoxin reductase 1	TXNRD1				32[g]	
Ubiquitin-like modifier activating enzyme 1	UBE1	UBA1[f]				
Ubiquitin-conjugating enzyme E2N	UBE2N	UBC13	106.5 ± 19.4			++
Tryptophanyl-tRNA synthetase	WARS	WRS1[f]			32[g]	+
Tyrosine 3-monooxygenase/tryptophan 5-monooxygenase activation protein, β polypeptide	YWHAB				32[g]	++
Tyrosine 3-monooxygenase/tryptophan 5-monooxygenase activation protein, ζ polypeptide	YWHAZ	BMH2	98.7 ± 20.7			++
Zinc and ring finger 2	ZNRF2					
Additional proteins associated to autophagosomal clusters						
CAP, adenylate cyclase-associated protein 1	CAP1	SRV2	**50.4 ± 11.1**	**42.4 ± 10.4**		++
Vacuolar protein sorting 35 homolog	VPS35	VPS35	**12.4 ± 3.2**	**36.3 ± 21.1**		++

[a] As measured by the alkaline phosphatase (ALP) activity assay. The values represent triplicates, and the standard deviations are indicated. The numbers marked in bold type indicate significant changes in the value obtained by ALP assay compared with randomly chosen control KO strains ($p < 0.05$, one-way analysis of variance).

[b] Nitrogen starvation (3 h).

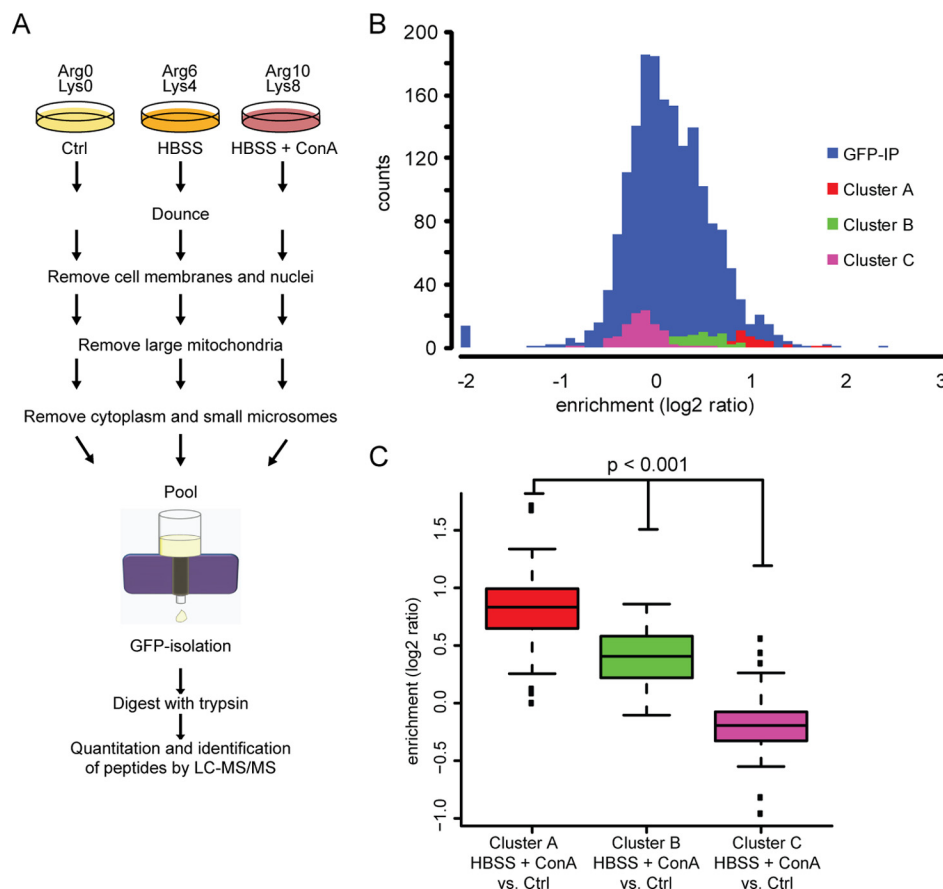[c] Rapamycin treatment (0.5 μg/ml; 3 h).

[d] Proteins previously described in autophagosomes are referenced.

[e] Identified in one (+) or two (++) eGFP-IPs of cells treated with HBSS or rapamycin in addition to concanamycin A.

[f] Knockout strain not viable.

[g] Autophagy-related proteins but so far not linked to the autophagosome are referenced.

[h] Rat ortholog.

FIG. 3. **Identification of proteins in immunopurified autophagosomes.** *A*, schematic diagram of the SILAC-based immunoprecipitation experiment performed to identify and quantify autophagosome associated proteins in HBSS- and ConA-treated (20 nM) cells (3 h) as compared with untreated cells. The lysate was centrifuged to enrich autophagosome-associated LC3 and to deplete the free pool of LC3 prior to affinity purification using anti-GFP antibody coated magnetic beads. *B*, graph showing the relative ratios of proteins identified in the affinity experiments (HBSS and ConA *versus* control, GFP-IP). Common proteins identified in clusters A–C from the PCP-SILAC experiment displayed nonrandom ratio distributions. *C*, common cluster A proteins are significantly enriched in immunopurified autophagosomes (HBSS and ConA *versus* control) as compared with common cluster B and C proteins (one-way analysis of variance, Tukey post hoc test). *Ctrl*, control.

tures whose composition is influenced by the nature and timing of the stress stimulus.

Autophagy Modulates Proteasomal Activity—Our findings suggest that the autophagic machinery and the proteasome are interconnected (Figs. 2*C* and 5*A*). Interplay between the two degradation systems has been proposed lately (24). However, because a detailed description of the connection of these two major cellular degradation pathways is still missing, we investigated their interplay in more detail. First, we confirmed the stimulus-independent partial co-localization of proteasomal proteins and LC3 by fluorescence microscopy and Western blot analyses (Fig. 6, *A–J*). This evidence of proteasomal 20 S subunits associated with autophagosomes led us to speculate whether autophagy might decrease the proteasome level in cells. Indeed, the abundance of proteasomal proteins in whole cell lysates decreased upon amino acid starvation, and importantly this decrease could be blocked by the addition of 3-methyladenine, an inhibitor of autophagy (40) (Fig. 6*K*). Accordingly, induction of autophagic flux by rapa-

mycin or starvation led to a significant decrease in proteasomal activity (Fig. 6*L*). Notably, concanamycin A, which inhibits the degradation of autophagosomal cargo (Fig. 5*C*), did not influence the proteasomal activity (Fig. 6*L*). Furthermore autophagosomes purified by immunoprecipitation of eGFP-LC3 with an anti-GFP antibody contained proteasomal subunits, supporting their association with autophagosomes. Interestingly, incubation of these purified autophagosomes with detergent abolished the pulldown of the proteasomal subunits. This suggests that the proteasomal subunits do not directly interact with LC3 but rather associate with the autophagosome. Contrary, p62 was pulled down with eGFP-LC3 independent of detergent treatment as expected (Fig. 6*M*). Taken together, these data suggest that the proteasome associates with autophagosomes independently of LC3 and that functional autophagy leads to a decrease in proteasome amount and activity.

Functional Analysis of Common Autophagosome-associated Proteins—Our experimental setup did not allow us to

FIG. 4. **Validation of autophagosomal localization of p62, RHEB and FKBP1A.** MCF7 cells expressing eGFP-LC3 (*A*), DsRed-RHEB (*B*), or FKBP1A-DsRed (*C*) were treated for 7 h with 2 nM concanamycin A and stained with anti-p62 (*A*) or anti-LC3-antibody (*B* and *C*). *Yellow* staining indicating co-localization of LC3 puncta and candidate proteins was observed in all three cases (*scale bars*, 20 μm). Fluorophore profiles of co-localization are shown in supplemental Figs. S4 and S5. PCP-SILAC profiles of the respective proteins closely follow the MAP1LC3B profiles shown in Fig. 1*E*.
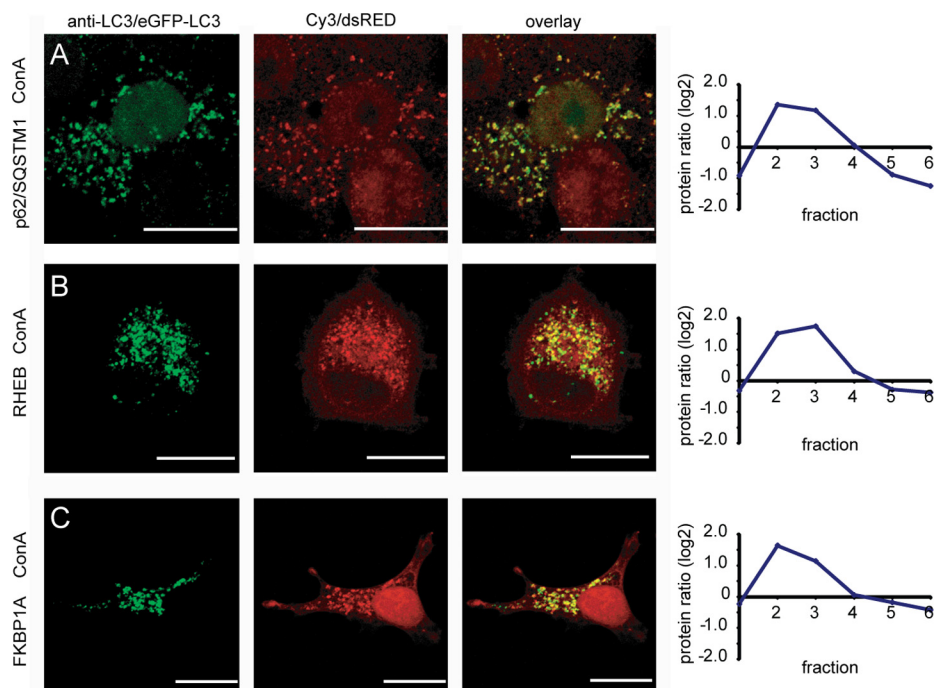
directly distinguish between cargo and core proteins. p62 is required for starvation-induced LC3 translocation (41), and we speculated whether other candidates involved in autophagy regulation are among the 94 common autophagosome-associated proteins. To investigate this further, we performed an ortholog screen in the yeast *Saccharomyces cerevisiae* whose genome contains 59 orthologs of the human genes encoding for the 94 common autophagosome-associated proteins, giving rise to 32 viable knock-out strains (Table I). In addition, we included two proteins involved in vesicle trafficking, CAP1 and VPS35, which were present in one or two of the three autophagosomal clusters, enriched in the autophagosome pull-downs and also giving rise to viable yeast knock-out strains. All of the strains were starved and tested for their autophagic response by the ALP assay (29) indicative of autophagic flux (Fig. 7*A*). Strains deficient in the yeast orthologs of mammalian CAP1 (*SRV2*), EEF1G (*TEF4*), LC3 (*ATG8*), NP (*PNP1*), RHEB (*RHB1*), and VPS35 (*VPS35*) had significantly lower autophagic activity, whereas the yeast strain deficient in the ortholog of mammalian GNB2L1 (*ASC1*) had significantly higher autophagic activity upon starvation as compared with the wild-type strain (Fig. 7*A*). Except for the yeast strain deficient for *TEF4*, similar changes in the autophagic flux were observed when autophagy was triggered by rapamycin treatment (Fig. 7*B*).

The strong phenotype observed for the vacuolar protein sorting protein VPS35 suggested a so far unknown role of the retromer complex in autophagy. This complex mediates retrograde transport of cargo from endosomes to the trans Golgi network and is composed of the cargo selective subunits VPS26, VPS29, and VPS35 and the sorting nexin subunits VPS5 and VPS17 (42). To corroborate the phenotype data for VPS35, we analyzed additional subunits of the retromer complex. Interestingly, strains deficient for the subunits VPS29, VPS5, and VPS17 revealed equally low autophagic activity in cells starved or treated with rapamycin. These data further support that the retromer complex is required for TOR-dependent autophagy in yeast (Fig. 7*C*).

To test whether the autophagy regulating functions of the yeast proteins were conserved in mammalian cells, we depleted MCF7 cells for the ortholog proteins using RNA interference and measured the level of p62 in control conditions and following autophagy induction by amino acid starvation or etoposide treatment, which we have used recently to establish a luciferase-based autophagy screen (30) (Fig. 7*D*). No major differences in p62 levels in control conditions were observed upon siRNA-mediated depletion of CAP1, GNB2L1, or VPS35, whereas depletion of RHEB reduced the cellular p62 level, suggesting that RHEB siRNA induced spontaneous autophagy (Fig. 7*D* and data not shown). Accordingly, two nonoverlapping RHEB siRNAs increased the autophagic flux as measured by a decrease in the ratio of RLuc-LC3-WT/RLuc-LC3^{G120A} (30) (Fig. 7*E*) and increased the number of cells with eGFP-LC3 translocation (Fig. 7*F*). As expected for the control experiments, the induction of autophagy by amino acid starvation and etoposide decreased the level of p62, and etoposide decreased the ratio of RLuc-LC3-WT/RLuc-LC3^{G120A} and increased the number of cells with eGFP-LC3 translocation in cells treated with control siRNA (Fig. 7, *D–F*). All of these changes indicative of autophagy were inhibited in cells depleted for EEF1G by two nonoverlapping siRNAs (Fig. 7, *D–F*, and data not shown). Interestingly, depletion of EEF1G
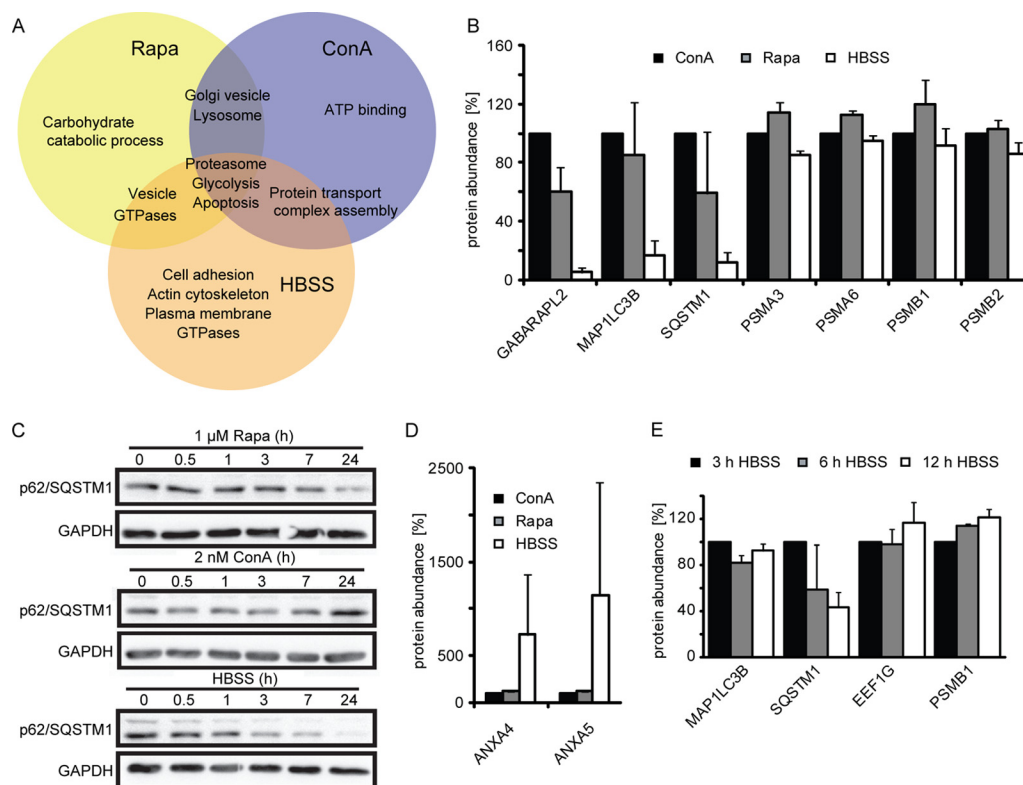
FIG. 5. **Autophagosome-associated protein dynamics.** *A*, comparison of cluster A proteins identified by PCP-SILAC indicates stimuli-dependent autophagosome-protein association for Rapa- and ConA-treated and starved cells based on Gene Ontology analysis. *B*, direct comparison of autophagosome-associated proteins by SILAC-based quantitative analysis of autophagosomes isolated from MCF7 cells treated with 100 nM Rapa or 2 nM ConA or starved in HBSS for 7 h and mixed in a ratio of 1:1:1. The relative abundance of proteins per autophagosome is normalized to the ConA isotope signal. Shown are the combined results from two biological replicates. *C*, p62 levels in MCF7 cells treated with 1 μM Rapa or 2 nM ConA or starved in HBSS for the indicated time periods were analyzed by immunoblotting using GAPDH as loading control. *D*, relative abundances of indicated annexins in autophagosomes from cells treated and analyzed as in *B*. Shown are the combined results from two biological replicates. *E*, autophagosome-associated protein dynamics. Autophagosomes were isolated from SILAC labeled cells and combined in a ratio of 1:1:1 after starvation for 3, 6, and 12 h. Protein-dependent targeting dynamics was observed. Shown are the combined results from two biological replicates.

also attenuated etoposide- and starvation-induced inhibition of mTORC1 as measured by levels of p70S6K phosphorylation (supplemental Fig. S6). Autophagy induced by starvation but not that induced by rapamycin is defective in yeast deficient for the EEF1G ortholog TEF4 (Fig. 7, *A* and *B*). This suggests that EEF1G is a positive regulator of autophagy required for autophagy signaling upstream of mTORC1.

DISCUSSION

The data presented above provide a framework of autophagosome-associated proteins and will help in characterizing underlying cellular processes regulating the biogenesis and cargo selection of autophagosomes. Employing PCP-SILAC, we grouped the identified proteins in three clusters per organelle preparation for cells treated with concanamycin A, rapamycin, and HBSS. The clusters consisted of autophagosomal candidate proteins (cluster A); proteins found both in autophagosomal fractions and in other organelles such as endolysosomes, ER, and Golgi apparatus (cluster B); and nonautophagosomal proteins such as ER and nuclear pro-

teins (cluster C). For further investigations, we concentrated on proteins observed in cluster A.

The most comprehensive proteomic analysis of autophagosomes prior to this study identified 39 and 101 proteins localizing to autophagosomal membranes in starved rat hepatocytes and human cell lines, respectively (33, 34). We chose a different approach characterizing not only autophagosomal membrane proteins but also autophagosomal cargo proteins to learn more about cellular proteome dynamics during autophagy. With this approach, we identified 728 autophagosomal candidate proteins, of which 94 were found in the autophagosome cluster regardless of the stimulus. Our data suggest that 31 proteins previously linked to autophagy are also associated with the autophagosome, among them the proteasome.

Comparison of the 94 common proteins with the other two reported data sets revealed seven human ortholog proteins shared with the autophagosomal rat proteins identified by Øverbye *et al.* (34) and a single protein shared with the 101 identified by Gao *et al.* (33). The rather small overlap might reflect differences in stimuli, isolation procedures, cell types,
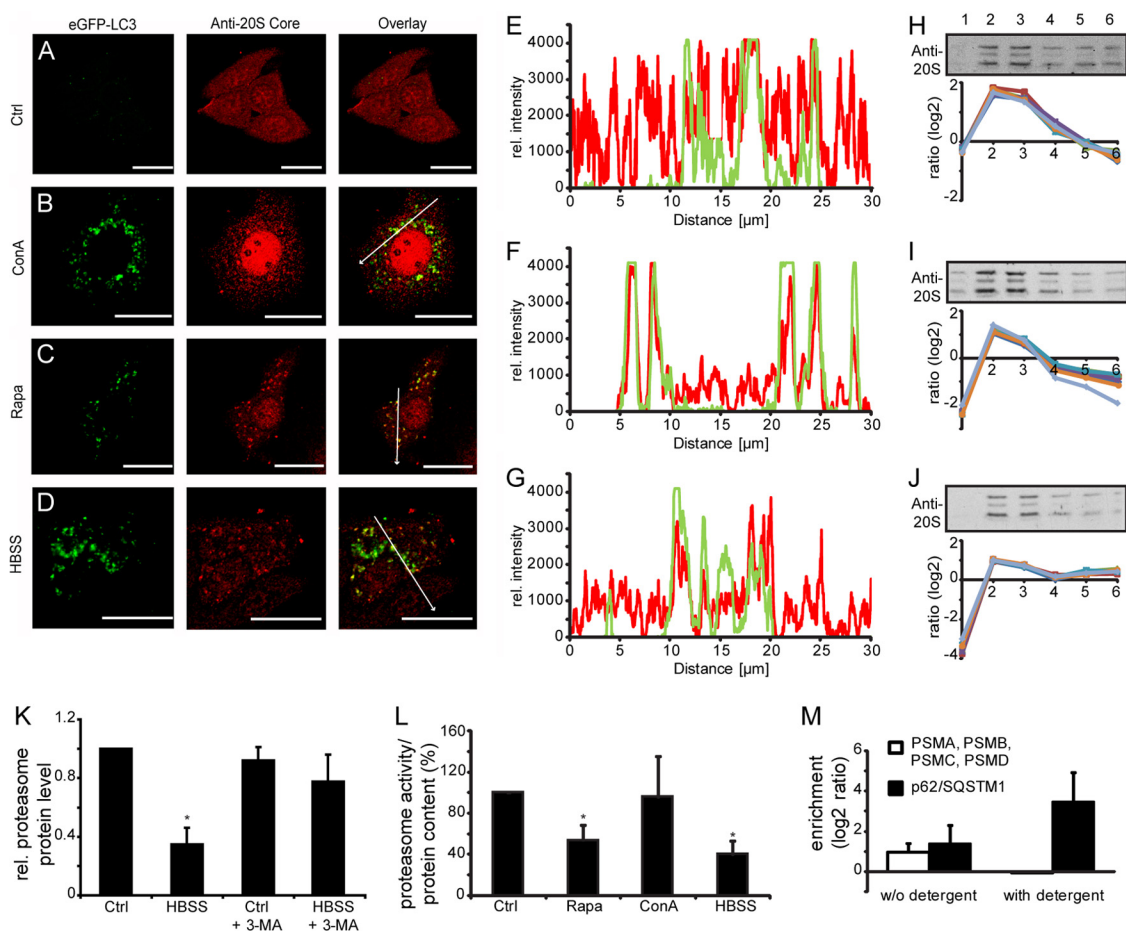
FIG. 6. **Targeting of the proteasome to autophagosomes.** *A–D*, 20 S core proteasome subunits were visualized using a polyclonal antibody in MCF7-eGFP-LC3 cells left untreated (control) or treated for 7 h with 2 nM ConA or 100 nM Rapa or starved for amino acids in HBSS. Whereas untreated control cells show an evenly distributed staining (*A*), autophagosome-protein co-localization can be detected in autophagy-induced cells (*B–D*). *Scale bars*, 20 μm. *E–G*, partial co-localization of proteasomes and autophagosomes after induction of autophagy were observed from profiles of relative intensities of the two fluorophores along the respective *white lines* marked in *B–D*. *H–J*, PCP-SILAC profiles of proteasomal proteins were validated by Western blot analyses of biological replicates (ConA, Rapa, and HBSS). Shown are bands for the 20 S core subunits, which follow the MS profiles in all three stimuli. *K*, the relative abundance of proteasomal subunits were determined by SILAC-based mass spectrometry of cells left untreated or starved for 12 h with or without 10 mM 3-methyladenine combined in a ratio of 1:1. Shown are the relative changes compared with control cells (average ratio of detected PSMA, PSMB, PSMC, and PSMD proteins; the *error bars* indicate standard deviations). *, $p < 0.01$ as analyzed by a one-sample *t* test. *L*, changes in proteasome activity in response to autophagy were analyzed in lysates of MCF7 cells left untreated (control) or treated for 24 h with 2 nM ConA or 1 μM Rapa or starved for amino acids in HBSS. The values are percentages of proteasome activity/protein concentration as compared with untreated control samples and represent the averages ± S.D. from four independent experiments. *, $p < 0.01$ as analyzed by a one-sample *t* test. *M*, proteasome association with LC3 affinity-purified autophagosomes was analyzed by SILAC-based mass spectrometry using MCF7-eGFP-LC3 cells left untreated (control) or stimulated with 2 nM ConA for 7 h. Anti-GFP immunoprecipitations were performed in lysis buffer with or without 1% Nonidet P-40. Without detergent, intact autophagosomes were purified. Under these conditions, enrichment of proteasomal proteins (average ratio of detected PSMA, PSMB, PSMC, and PSMD proteins) was observed similar to p62/SQSTM1. In the presence of detergent, autophagosomes were destroyed, and the proteasomal proteins were no longer enriched in contrast to proteins binding directly to LC3 such as SQSTM1. The values represent the averages from two independent experiments ± S.D. *Ctrl*, control.

and MS methods. Whereas Øverbye *et al.* did not identify any of the known ATG proteins, we determined complete protein profiles of the two human ATG8 homologs, MAP1LC3B and GABARAPL2. Gao *et al.* identified MAP1LC3B, ATG7 and ATG9. We identified ATG3 and ATG4B and detected single peptides from ATG9A and ATG5. The abundance of the latter proteins was too low for the extraction of complete protein profiles, and therefore they were omitted from further analysis.

However, the partial profiles of these proteins closely resemble the profiles of proteins in cluster A (data not shown), indicating that these ATGs may also localize to autophagosomes as suggested previously (43). Taken together, ATG proteins appear to be low abundant and are not commonly identified by large scale proteomics studies. For their analyses, dedicated affinity purification protocols appear to be more promising (32).
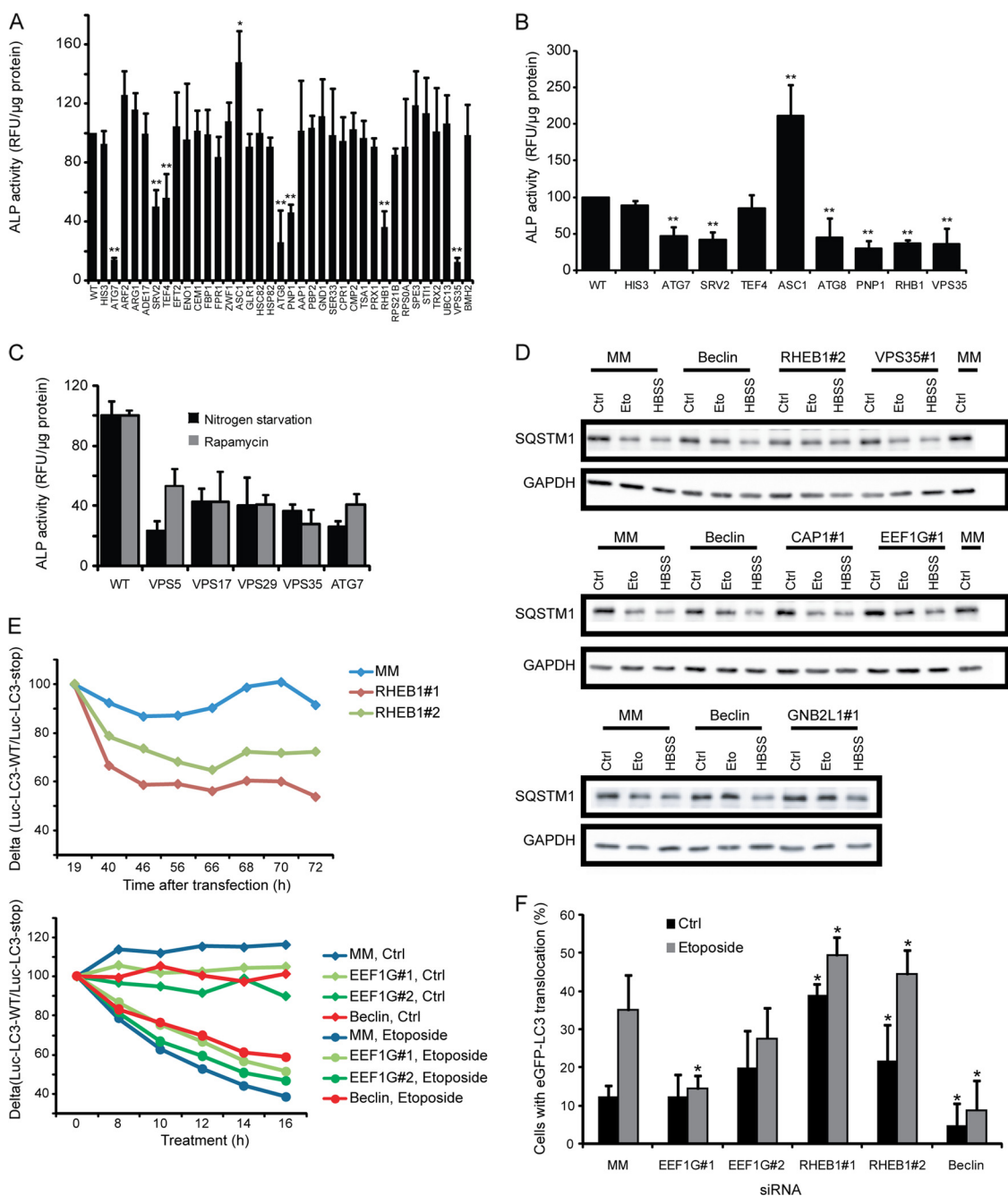
FIG. 7. **Genetic screens for novel autophagy regulators in yeast and mammalian cells.** *A* and *B*, ALP screen in *S. cerevisiae*. The ALP activity was measured in indicated *S. cerevisiae* knock-out strains starved for nitrogen (*A*) or treated with 500 ng/ml rapamycin (*B*) for 3 h. A histidine-dependent strain and an ATG7 knock-out strain were used as negative and positive controls, respectively. The values are percentages of ALP activity/μg protein as compared with the wild-type control strain and represent the averages $\pm$ S.D. from three independent experiments. *, $p < 0.05$; **, $p < 0.005$ as analyzed by one-way analysis of variance followed by a least significant difference post hoc test. *C*, functional analysis of yeast retromer subunits. The indicated retromer yeast knock-out strains were treated as in *A* and *B*. The values are percentages of ALP activity/μg protein as compared with the wild-type control strain and represent the averages $\pm$ S.D. from three independent experiments. An ATG7 knock-out strain was used as a positive control. *D*, immunoblot analysis of p62 and GAPDH (loading control) from lysates of MCF7-eGFP-LC3 cells 64 h after transfection with indicated siRNAs, which had been validated by QRT-PCR (data not shown). The cells were left untreated or treated with 50 μM etoposide or starved for amino acids for 16 or 8 h before harvesting, respectively. The experiment was repeated a minimum of three times with essentially same results. *E*, functional analysis of human candidate proteins. MCF7 cells stably expressing RLuc-LC3wt or RLuc-LC3^{G120A} were plated in separate wells of a 96-well dish and transfected with indicated siRNAs. In the *upper graph*, 50 nM EnduRen™ was added 17 h after the transfection, and the luciferase activities were measured at the indicated time points. For the *lower graph*, 50 nM EnduRen™ was added 54 h after transfection. Two hours later the luciferase activities were

By analyzing autophagosomes from cells undergoing stress-induced autophagy by amino acid starvation, rapamycin-induced autophagy, and basal autophagy, which was blocked by concanamycin A, we compared autophagosomes from cells under fundamental different conditions. These analyses revealed proteins that always appear to associate with autophagosomes and others that appear to associate in a cell condition-dependent manner. Hence, stress-induced macroautophagy appears to differ from basal macroautophagy, and further studies are needed to understand stimulus-dependent cargo recruitment to autophagosomes.

An interesting finding in our study was the association between the proteasome and the autophagosome. In the past, the proteasomal and the autophagosomal/lysosomal pathways have been regarded as discrete degradation routes. Lately, a closer connection became more likely (4, 24, 44), and it has been described that the proteasome can be degraded in lysosomes (45). However, no detailed analyses of the interplay between these two degradation pathways have been reported. Here, we show that the proteasome localizes to autophagosomes regardless of the three stimuli and that the amount and activity of the proteasome are significantly decreased by functional autophagy. It is surprising that the proteasome associates with autophagosomes as the overall protein degradation increases during autophagy. However, several possible reasons might exist. First, autophagy induction is often associated with cellular stress and decreased cell growth. Thus, the removal of the proteasome and the subsequent accumulation of proteasomal substrates such as cyclins may contribute to cell cycle arrest. We tested this hypothesis but were not able to detect increased levels of cyclin D in cell lysate after autophagy induction (data not shown). This might be due to several compensatory mechanisms: 1) inhibition of protein synthesis because of inhibition of mTORC1 during autophagy activation or 2) autophagy might degrade proteins normally removed by the proteasome, *e.g.* via removal of p62-ubiquitinated protein aggregates (22). Second, one of the major functions of autophagy is to preserve cellular energy and thus degradation of the excess proteasome, which is not needed in circumstances where autophagy is activated, and *de novo* protein synthesis minimized via the inhibition of mTORC1 may serve as an important source of energy and amino acids. Furthermore, the degradation of proteasome substrates in autolysosomes may be less energy demanding than proteolysis by the proteasome. Last but not least, the proteasome could "help" to degrade ubiquitinated/unfolded cargo in the autophagosome. In favor of this theory, several subunits of PSMA (subunits 2, 3, 5, 6,

and 7) and PSMB (subunits 1, 2, 3, 4, 5, 6 and 7) proteins were detected in the autophagosome cluster. Because these subunits form the "active proteasome," the functional proteasome complex appears to be autophagosomal cargo. This is further supported by the detection of protein-conjugated ubiquitin in autophagosomes by PCP-SILAC, immunofluorescence, and Western blot (data not shown) and by the fact that the proteasome activity is not decreased in concanamycin A-treated cells even though autophagosomes containing proteasomes accumulate in these cells.

Our data suggest that there is a balance between the two degradation systems that can be shifted in favor of one or the other, in our case active autophagy leading to reduced proteasome activity. In support of this notion, we observed increased levels of rapamycin-induced autophagy in yeast when the proteasome was inactivated by temperature-sensitive pre1-1 or pre2-1 mutants. The pre1-1/2-1 double mutant displayed synergistic effects (supplemental Fig. S7). Enhanced autophagy upon proteasome impairment suggests a compensatory mechanism as reported previously (21).

Among the new autophagosomal candidate proteins, we identified six autophagy regulators by a functional yeast screen that were not identified in the original screens characterizing *Atg* genes in yeast (46). This difference might be due to different screening methods. The original paper identified mutants defective in nitrogen starvation-induced autophagy as clones that lost viability faster than wild-type cells and were defective in accumulation of autophagic bodies in the vacuole. In contrast, we used the ALP assay. The orthologs of mammalian CAP1, EEF1G, RHEB, NP, and VPS35 were required for starvation-induced autophagy, whereas the yeast strain lacking the ortholog of mammalian GNB2L1 showed an increased autophagic response compared with the wild-type strain. Interestingly, testing additional subunits of the retromer complex revealed the same phenotype initially observed for the VPS35 subunit. In addition, the subunit VPS26 associated with autophagosomes in starved cells as identified by PCP-SILAC and anti-eGFP pulldowns. These data suggest that the retromer complex and retrograde transport play a role in autophagy, possibly by delivering vesicles or recycling autophagosomal membrane proteins.

Applying siRNA knockdown in human cells, we observed a change in the autophagic response after depleting cells for EEF1G or RHEB. Although we did not observe any major changes in the level of autophagy in cells depleted for CAP1, VPS35, and GNB2L1, we cannot exclude that these might have an effect if a more efficient down-regulation was

measured ($T = 0$), the cells were left untreated (control) or treated with 50 μM etoposide, and the luciferase activities were measured at the indicated time points. The experiment was repeated five times with similar results. *F*, functional analysis of human candidate proteins. MCF7-eGFP-LC3 cells were left untreated or treated with 50 μM etoposide for 6 h. Histograms with percentages of green cellular cross-sections with over five LC3-positive dots are shown. The values represent the means $\pm$ S.D. from three to six independent experiments. *, p value < 0.05 analyzed by a two-tailed unpaired *t* test. *Ctrl*, control; *WT*, wild type; *MM*, mock treated control.

achieved. As expected, the mTORC1 activator RHEB constitutively blocked autophagy in human cells. The fact that we identify it as an autophagosomal protein fits with our recent data showing that starvation induces its degradation (19, 47). Therefore, removal of RHEB by autophagy might serve as a positive feedback mechanism to ensure a massive autophagy response. Surprisingly, the ortholog of RHEB in yeast was found to be required for both starvation- and rapamycin-induced autophagy. This controversy could be explained by the fact that contrary to mammals, which have two RHEB isoforms, yeast only has one RHEB isoform (RHB), which is only distantly related to mammalian RHEBs and whose knock-out does not affect the activity of TOR (48). Interestingly, EEF1G was found to be a universal autophagy regulator. Similar to LC3 it locates in/at the autophagosomes and is required for the process. However, contrary to LC3, it functions upstream of mTORC1. The exact molecular mechanism whereby EEF1G regulates mTORC1 activity remains to be revealed.

In summary, the analysis of organellar protein composition in our study highlights the complex character of autophagy shedding light on an elemental metabolic pathway that we are only starting to comprehend. The catalog of autophagosome-related proteins assembled from PCP-SILAC data and cross-examined by autophagosome immunoprecipitations revealed interplay between the autophagosome and the proteasome systems. In addition, we identified novel autophagosomal components of which EEF1G was found to be an autophagy regulator in both yeast and human cells.

REFERENCES

1. Kroemer, G., and Jäättelä, M. (2005) Lysosomes and autophagy in cell death control. *Nat. Rev. Cancer* **5,** 886–897
2. Mizushima, N., Levine, B., Cuervo, A. M., and Klionsky, D. J. (2008) Autophagy fights disease through cellular self-digestion. *Nature* **451,** 1069–1075
3. Nakatogawa, H., Suzuki, K., Kamada, Y., and Ohsumi, Y. (2009) Dynamics and diversity in autophagy mechanisms: Lessons from yeast. *Nat. Rev. Mol. Cell Biol.* **10,** 458–467
4. Engelke, R., Becker, A. C., and Dengjel, J. (2012) The degradative inventory of the cell: Proteomic insights. *Antioxid. Redox Signal.*, doi: 10.1089/ars.2011.4393
5. Tsukamoto, S., Kuma, A., Murakami, M., Kishi, C., Yamamoto, A., and Mizushima, N. (2008) Autophagy is essential for preimplantation development of mouse embryos. *Science* **321,** 117–120
6. Kuma, A., Hatano, M., Matsui, M., Yamamoto, A., Nakaya, H., Yoshimori, T., Ohsumi, Y., Tokuhisa, T., and Mizushima, N. (2004) The role of autophagy during the early neonatal starvation period. *Nature* **432,** 1032–1036
7. Rubinsztein, D. C. (2006) The roles of intracellular protein-degradation pathways in neurodegeneration. *Nature* **443,** 780–786
8. Mathew, R., Karantza-Wadsworth, V., and White, E. (2007) Role of autophagy in cancer. *Nat. Rev. Cancer* **7,** 961–967
9. Gordon, P. B., and Seglen, P. O. (1988) Prelysosomal convergence of autophagic and endocytic pathways. *Biochem. Biophys. Res. Commun.* **151,** 40–47
10. Finn, P. F., and Dice, J. F. (2006) Proteolytic and lipolytic responses to starvation. *Nutrition* **22,** 830–844
11. Klionsky, D. J., Cregg, J. M., Dunn, W. A., Jr., Emr, S. D., Sakai, Y., Sandoval, I. V., Sibirny, A., Subramani, S., Thumm, M., Veenhuis, M., and Ohsumi, Y. (2003) A unified nomenclature for yeast autophagy-related genes. *Dev. Cell* **5,** 539–545
12. Ohsumi, Y. (2001) Molecular dissection of autophagy: Two ubiquitin-like systems. *Nat. Rev. Mol. Cell Biol.* **2,** 211–216
13. Yang, Z., and Klionsky, D. J. (2010) Mammalian autophagy: Core molecular machinery and signaling regulation. *Curr. Opin. Cell Biol.* **22,** 124–131
14. Kim, I., Rodriguez-Enriquez, S., and Lemasters, J. J. (2007) Selective degradation of mitochondria by mitophagy. *Arch. Biochem. Biophys.* **462,** 245–253
15. Bernales, S., McDonald, K. L., and Walter, P. (2006) Autophagy counterbalances endoplasmic reticulum expansion during the unfolded protein response. *PLoS Biol.* **4,** e423
16. Dunn, W. A., Jr., Cregg, J. M., Kiel, J. A., van der Klei, I. J., Oku, M., Sakai, Y., Sibirny, A. A., Stasyk, O. V., and Veenhuis, M. (2005) Pexophagy: The selective autophagy of peroxisomes. *Autophagy* **1,** 75–83
17. Kraft, C., Deplazes, A., Sohrmann, M., and Peter, M. (2008) Mature ribosomes are selectively degraded upon starvation by an autophagy pathway requiring the Ubp3p/Bre5p ubiquitin protease. *Nat. Cell Biol.* **10,** 602–610
18. Pohl, C., and Jentsch, S. (2009) Midbody ring disposal by autophagy is a post-abscission event of cytokinesis. *Nat. Cell Biol.* **11,** 65–70
19. Kristensen, A. R., Schandorff, S., Høyer-Hansen, M., Nielsen, M. O., Jäättelä, M., Dengjel, J., and Andersen, J. S. (2008) Ordered organelle degradation during starvation-induced autophagy. *Mol. Cell. Proteomics* **7,** 2419–2428
20. Ciechanover, A. (2005) Proteolysis: From the lysosome to ubiquitin and the proteasome. *Nat. Rev. Mol. Cell Biol.* **6,** 79–87
21. Pandey, U. B., Nie, Z., Batlevi, Y., McCray, B. A., Ritson, G. P., Nedelsky, N. B., Schwartz, S. L., DiProspero, N. A., Knight, M. A., Schuldiner, O., Padmanabhan, R., Hild, M., Berry, D. L., Garza, D., Hubbert, C. C., Yao, T. P., Baehrecke, E. H., and Taylor, J. P. (2007) HDAC6 rescues neurodegeneration and provides an essential link between autophagy and the UPS. *Nature* **447,** 859–863
22. Korolchuk, V. I., Mansilla, A., Menzies, F. M., and Rubinsztein, D. C. (2009) Autophagy inhibition compromises degradation of ubiquitin-proteasome pathway substrates. *Mol. Cell* **33,** 517–527
23. Kraft, C., Peter, M., and Hofmann, K. (2010) Selective autophagy: Ubiquitin-mediated recognition and beyond. *Nat. Cell Biol.* **12,** 836–841
24. Lamark, T., and Johansen, T. (2010) Autophagy: Links with the proteasome. *Curr. Opin. Cell Biol.* **22,** 192–198
25. Zimmermann, A. C., Zarei, M., Eiselein, S., and Dengjel, J. (2010) Quanti-

tative proteomics for the analysis of spatio-temporal protein dynamics during autophagy. *Autophagy* **6,** 1009–1016

26. Andersen, J. S., Wilkinson, C. J., Mayor, T., Mortensen, P., Nigg, E. A., and Mann, M. (2003) Proteomic characterization of the human centrosome by protein correlation profiling. *Nature* **426,** 570–574

27. Dengjel, J., Kratchmarova, I., and Blagoev, B. (2009) Receptor tyrosine kinase signaling: A view from quantitative proteomics. *Mol. Biosyst.* **5,** 1112–1121

28. Ong, S. E., Blagoev, B., Kratchmarova, I., Kristensen, D. B., Steen, H., Pandey, A., and Mann, M. (2002) Stable isotope labeling by amino acids in cell culture, SILAC, as a simple and accurate approach to expression proteomics. *Mol. Cell. Proteomics* **1,** 376–386

29. Klionsky, D. J. (2007) Monitoring autophagy in yeast: The Pho8Delta60 assay. *Methods Mol. Biol.* **390,** 363–371

30. Farkas, T., Hoyer-Hansen, M., and Jaattela, M. (2009) Identification of novel autophagy regulators by a luciferase-based assay for the kinetics of autophagic flux. *Autophagy* **5,** 1018–1025

31. Klionsky, D. J., Klionsky, D. J., Abeliovich, H., Agostinis, P., Agrawal, D. K., Aliev, G., Askew, D. S., Baba, M., Baehrecke, E. H., Bahr, B. A., Ballabio, A., Bamber, B. A., Bassham, D. C., Bergamini, E., Bi, X., Biard-Piechac-zyk, M., Blum, J. S., Bredesen, D. E., Brodsky, J. L., Brumell, J. H., Brunk, U. T., Bursch, W., Camougrand, N., Cebollero, E., Cecconi, F., Chen, Y., Chin, L. S., Choi, A., Chu, C. T., Chung, J., Clarke, P. G., Clark, R. S., Clarke, S. G., Clavé, C., Cleveland, J. L., Codogno, P., Colombo, M. I., Coto-Montes, A., Cregg, J. M., Cuervo, A. M., Debnath, J., Demar-chi, F., Dennis, P. B., Dennis, P. A., Deretic, V., Devenish, R. J., Di Sano, F., Dice, J. F., Difiglia, M., Dinesh-Kumar, S., Distelhorst, C. W., Djava-heri-Mergny, M., Dorsey, F. C., Dröge, W., Dron, M., Dunn, W. A., Jr., Duszenko, M., Eissa, N. T., Elazar, Z., Esclatine, A., Eskelinen, E. L., Fésüs, L., Finley, K. D., Fuentes, J. M., Fueyo, J., Fujisaki, K., Galliot, B., Gao, F. B., Gewirtz, D. A., Gibson, S. B., Gohla, A., Goldberg, A. L., Gonzalez, R., González-Estévez, C., Gorski, S., Gottlieb, R. A., Häussinger, D., He, Y. W., Heidenreich, K., Hill, J. A., Høyer-Hansen, M., Hu, X., Huang, W. P., Iwasaki, A., Jäättelä, M., Jackson, W. T., Jiang, X., Jin, S., Johansen, T., Jung, J. U., Kadowaki, M., Kang, C., Kelekar, A., Kessel, D. H., Kiel, J. A., Kim, H. P., Kimchi, A., Kinsella, T. J., Kiselyov, K., Kitamoto, K., Knecht, E., Komatsu, M., Kominami, E., Kondo, S., Kovács, A. L., Kroemer, G., Kuan, C. Y., Kumar, R., Kundu, M., Landry, J., Laporte, M., Le, W., Lei, H. Y., Lenardo, M. J., Levine, B., Lieberman, A., Lim, K. L., Lin, F. C., Liou, W., Liu, L. F., Lopez-Berestein, G., López-Otín, C., Lu, B., Macleod, K. F., Malorni, W., Martinet, W., Matsuoka, K., Mautner, J., Meijer, A. J., Meléndez, A., Michels, P., Miotto, G., Mistiaen, W. P., Mizushima, N., Mograbi, B., Monastyrska, I., Moore, M. N., Moreira, P. I., Moriyasu, Y., Motyl, T., Münz, C., Murphy, L. O., Naqvi, N. I., Neufeld, T. P., Nishino, I., Nixon, R. A., Noda, T., Nürnberg, B., Ogawa, M., Oleinick, N. L., Olsen, L. J., Ozpolat, B., Paglin, S., Palmer, G. E., Papassideri, I., Parkes, M., Perlmutter, D. H., Perry, G., Piacentini, M., Pinkas-Kramarski, R., Prescott, M., Proikas-Cezanne, T., Raben, N., Rami, A., Reggiori, F., Rohrer, B., Rubinsztein, D. C., Ryan, K. M., Sadoshima, J., Sakagami, H., Sakai, Y., Sandri, M., Sasakawa, C., Sass, M., Schneider, C., Seglen, P. O., Seleverstov, O., Settleman, J., Shacka, J. J., Shapiro, I. M., Sibirny, A., Silva-Zacarin, E. C., Simon, H. U., Simone, C., Simonsen, A., Smith, M. A., Spanel-Borowski, K., Srinivas, V., Steeves, M., Stenmark, H., Stromhaug, P. E., Subauste, C. S., Sugimoto, S., Sulzer, D., Suzuki, T., Swanson, M. S., Tabas, I., Takeshita, F., Talbot, N. J., Tallóczy, Z., Tanaka, K., Tanaka, K., Tanida, I., Taylor, G. S., Taylor, J. P., Terman, A., Tettamanti, G., Thompson, C. B., Thumm, M., Tolkovsky, A. M., Tooze, S. A., Truant, R., Tumanovska, L. V., Uchiyama, Y., Ueno, T., Uzcátegui, N. L., van der Klei, I., Vaquero, E. C., Vellai, T., Vogel, M. W., Wang, H. G., Webster, P., Wiley, J. W., Xi, Z., Xiao, G., Yahalom, J., Yang, J. M., Yap, G., Yin, X. M., Yoshimori, T., Yu, L., Yue, Z., Yuzaki, M., Zabirnyk, O., Zheng, X., Zhu, X., and Deter, R. L. (2008) Guidelines for the use and interpretation of assays for monitoring autophagy in higher eukaryotes. *Autophagy* **4,** 151–175

32. Behrends, C., Sowa, M. E., Gygi, S. P., and Harper, J. W. (2010) Network organization of the human autophagy system. *Nature* **466,** 68–76

33. Gao, W., Kang, J. H., Liao, Y., Ding, W. X., Gambotto, A. A., Watkins, S. C., Liu, Y. J., Stolz, D. B., and Yin, X. M. (2010) Biochemical isolation and characterization of the tubulovesicular LC3-positive autophagosomal compartment. *J. Biol. Chem.* **285,** 1371–1383

34. Øverbye, A., Fengsrud, M., and Seglen, P. O. (2007) Proteomic analysis of

membrane-associated proteins from rat liver autophagosomes. *Autophagy* **3,** 300–322

35. Andersen, J. S., and Mann, M. (2006) Organellar proteomics: Turning inventories into insights. *EMBO Rep.* **7,** 874–879

36. Jakobsen, L., Vanselow, K., Skogs, M., Toyoda, Y., Lundberg, E., Poser, I., Falkenby, L. G., Bennetzen, M., Westendorf, J., Nigg, E. A., Uhlen, M., Hyman, A. A., and Andersen, J. S. (2011) Novel asymmetrically localizing components of human centrosomes identified by complementary proteomics methods. *EMBO J.* **30,** 1520–1535

37. Blagoev, B., and Mann, M. (2006) Quantitative proteomics to study mitogen-activated protein kinases. *Methods* **40,** 243–250

38. Futschik, M. E., and Carlisle, B. (2005) Noise-robust soft clustering of gene expression time-course data. *J. Bioinform. Comput. Biol.* **3,** 965–988

39. Ashburner, M., Ball, C. A., Blake, J. A., Botstein, D., Butler, H., Cherry, J. M., Davis, A. P., Dolinski, K., Dwight, S. S., Eppig, J. T., Harris, M. A., Hill, D. P., Issel-Tarver, L., Kasarskis, A., Lewis, S., Matese, J. C., Richardson, J. E., Ringwald, M., Rubin, G. M., and Sherlock, G. (2000) Gene ontology: Tool for the unification of biology. The Gene Ontology Consortium. *Nat. Genet.* **25,** 25–29

40. Seglen, P. O., and Gordon, P. B. (1982) 3-Methyladenine: Specific inhibitor of autophagic/lysosomal protein degradation in isolated rat hepatocytes. *Proc. Natl. Acad. Sci. U.S.A.* **79,** 1889–1892

41. Bjørkøy, G., Lamark, T., Brech, A., Outzen, H., Perander, M., Overvatn, A., Stenmark, H., and Johansen, T. (2005) p62/SQSTM1 forms protein aggregates degraded by autophagy and has a protective effect on huntingtin-induced cell death. *J. Cell Biol.* **171,** 603–614

42. Collins, B. M. (2008) The structure and function of the retromer protein complex. *Traffic* **9,** 1811–1822

43. Xie, Z., and Klionsky, D. J. (2007) Autophagosome formation: Core machinery and adaptations. *Nat. Cell Biol.* **9,** 1102–1109

44. Zhao, J., Brault, J. J., Schild, A., Cao, P., Sandri, M., Schiaffino, S., Lecker, S. H., and Goldberg, A. L. (2007) FoxO3 coordinately activates protein degradation by the autophagic/lysosomal and proteasomal pathways in atrophying muscle cells. *Cell Metab.* **6,** 472–483

45. Cuervo, A. M., Palmer, A., Rivett, A. J., and Knecht, E. (1995) Degradation of proteasomes by lysosomes in rat liver. *Eur. J. Biochem.* **227,** 792–800

46. Tsukada, M., and Ohsumi, Y. (1993) Isolation and characterization of autophagy-defective mutants of *Saccharomyces cerevisiae*. *FEBS Lett.* **333,** 169–174

47. Dengjel, J., Kristensen, A. R., and Andersen, J. S. (2008) Ordered bulk degradation via autophagy. *Autophagy* **4,** 1057–1059

48. Urano, J., Tabancay, A. P., Yang, W., and Tamanoi, F. (2000) The *Saccharomyces cerevisiae* Rheb G-protein is involved in regulating canavanine resistance and arginine uptake. *J. Biol. Chem.* **275,** 11198–11206

49. Høyer-Hansen, M., Bastholm, L., Szyniarowski, P., Campanella, M., Szabadkai, G., Farkas, T., Bianchi, K., Fehrenbacher, N., Elling, F., Rizzuto, R., Mathiasen, I. S., and Jäättelä, M. (2007) Control of macroautophagy by calcium, calmodulin-dependent kinase kinase-β, and Bcl-2. *Mol. Cell* **25,** 193–205

50. Kissová, I., Deffieu, M., Manon, S., and Camougrand, N. (2004) Uth1p is involved in the autophagic degradation of mitochondria. *J. Biol. Chem.* **279,** 39068–39074

51. Strømhaug, P. E., Berg, T. O., Fengsrud, M., and Seglen, P. O. (1998) Purification and characterization of autophagosomes from rat hepatocytes. *Biochem. J.* **335,** 217–224

52. Dengjel, J., Jakobsen, L., and Andersen, J. S. (2010) Organelle proteomics by label-free and SILAC-based protein correlation profiling. *Methods Mol. Biol.* **658,** 255–265

53. Zarei, M., Sprenger, A., Metzger, F., Gretzmeier, C., and Dengjel, J. (2011) Comparison of ERLIC-TiO2, HILIC-TiO2, and SCX-TiO2 for global phosphoproteomics approaches. *J. Proteome Res.* **10,** 3474–3483

54. Schandorff, S., Olsen, J. V., Bunkenborg, J., Blagoev, B., Zhang, Y., Andersen, J. S., and Mann, M. (2007) A mass spectrometry-friendly database for cSNP identification. *Nat. Methods* **4,** 465–466

55. Mortensen, P., Gouw, J. W., Olsen, J. V., Ong, S. E., Rigbolt, K. T., Bunkenborg, J., Cox, J., Foster, L. J., Heck, A. J., Blagoev, B., Andersen, J. S., and Mann, M. (2010) MSQuant, an open source platform for mass spectrometry-based quantitative proteomics. *J. Proteome Res.* **9,** 393–403

56. Cox, J., and Mann, M. (2008) MaxQuant enables high peptide identification rates, individualized p.p.b.-range mass accuracies and proteome-wide

protein quantification. *Nat. Biotechnol.* **26,** 1367–1372

57. Rigbolt, K. T., Vanselow, J. T., and Blagoev, B. (2011) GProX, a user-friendly platform for bioinformatics analysis and visualization of quantitative proteomics data. *Mol. Cell. Proteomics* 10.1074/mcp.O110.007450

58. Kabeya, Y., Mizushima, N., Yamamoto, A., Oshitani-Okamoto, S., Ohsumi, Y., and Yoshimori, T. (2004) LC3, GABARAP and GATE16 localize to autophagosomal membrane depending on form-II formation. *J. Cell Sci.* **117,** 2805–2812

59. Scott, R. C., Schuldiner, O., and Neufeld, T. P. (2004) Role and regulation of starvation-induced autophagy in the *Drosophila* fat body. *Dev. Cell* **7,** 167–178